

Identifying the Surface Charges and their Impact on Carrier Dynamics in Quantum-Dot Light-Emitting Diodes by Impedance Spectroscopy

Zhenghui Wu, Pai Liu, Xiangwei Qu, Jingrui Ma, Wenbo Liu, Bing Xu, Kai Wang, and Xiao Wei Sun*

The carrier injection and charge transfer at interfaces in quantum dot light-emitting diodes (QLEDs) are commonly evaluated based on the energy levels of different functional layers. However, the actual charge dynamics in the experiments are found to be very different from the common expectations. In this work, QLEDs using 2,2'',2'''-(1,3,5-Benzinetriyl)-tris(1-phenyl-1-*H*-benzimidazole) (TPBi) or zinc oxide (ZnO) nanoparticles as electron transport layer (ETL) are studied by impedance spectroscopy. It was the first time to observe that the hole injection and electron injection start at different applied bias. In QLEDs with TPBi ETL, at an applied bias as low as 0.5 V, large amounts of holes have injected into the hole transport layer, while electron injection only occurs after the applied bias increased up to about 3.0 V. This is caused by the intrinsic accumulated negative charges in the quantum dot (QD) layer. The adverse impacts of the negative accumulated charges in QD layer are mitigated by replacing TPBi with ZnO. Hole injection and electron injection start at the same applied bias, or 1.7 V if ZnO replaces TPBi. Charge transfer and neutralization processes between QD and ZnO layers are adopted to explain the above results.

1. Introduction

Through numerous efforts on engineering of materials and devices, different types of high performance QLEDs were

achieved in recent five years.^[1–4] To understanding the limiting factors on the efficiency and stability of QLEDs, the optoelectronic properties of QD thin films, single QDs, and QD solutions have been studied by different kinds of optical spectroscopies.^[5–7] Indeed, a lot of problems observed in QLEDs were verified to correlate to the properties of QDs, such as lattice match between core and shell, and shell thicknesses.^[8–10] However, some physical processes in working devices cannot be understood by just separately characterizing individual components. Charge injection and transfer are examples of such key physical processes in QLEDs. Previous studies on charge injection in devices were mainly focused on the optoelectronic properties of the charge injection or transport layers.^[4,11] For example, the effects of surface-modified ZnO or doped ZnO on charge injection in QLEDs were intensively studied in


recent years.^[12,13] Jin and co-workers' most recent work deciphered the processes of charge injection and exciton formation in single-dot QLED.^[14] However, in the single-dot QLED, there are no interactions between QDs and the possible charge transfers between different functional layers are minimal, which suggest the actual charge dynamics in working devices may still be different. Our recent experimental phenomena revealed that the properties of QDs themselves including the degree of quantum confinement and surface traps made significant differences on carrier dynamics in QLEDs.^[9,15] The study on the actual carrier dynamics in working devices have not been sufficiently understood since they are too complicated and people usually focus on characterizing the functional layers separately.

Impedance spectroscopy was a very popular technique to study the charge dynamics in organic light-emitting diodes (OLEDs),^[16–19] while it was not quite often used in the studies of QLEDs. Uddin and Teo conducted impedance spectroscopy to demonstrate a layer of QDs sandwiched between two organic semiconductor layers increased the device capacitance.^[20] This was explained by the surface traps in QDs. More recently, Blauth et al. showed the negative capacitance in QLEDs and explained that it was due to the non-luminescent recombination at the trap sites in QD layer.^[21] Just in earlier

Dr. Z. Wu, Dr. P. Liu, X. Qu, J. Ma, W. Liu, Dr. B. Xu, Prof. K. Wang, Prof. X. W. Sun
Guangdong University Key Laboratory for Advanced Quantum Dot Displays and Lighting
Guangdong-Hong Kong-Macao Joint Laboratory for Photonic-Thermal-Electrical Energy Materials and Devices
Department of Electrical and Electronic Engineering
Southern University of Science and Technology
Shenzhen 518055, China
E-mail: sunxw@sustech.edu.cn

Dr. Z. Wu, Dr. P. Liu, Prof. K. Wang, Prof. X. W. Sun
Key Laboratory of Energy Conversion and Storage Technologies (Southern University of Science and Technology)
Ministry of Education
Shenzhen 518055, China

Dr. B. Xu, Prof. K. Wang, Prof. X. W. Sun
Shenzhen Planck Innovation Technologies Pte Ltd
Huan Cheng South Road, Longgang, Shenzhen 518129, China

 The ORCID identification number(s) for the author(s) of this article can be found under <https://doi.org/10.1002/adom.202100389>.

DOI: 10.1002/adom.202100389

days in this year, Kim and co-workers reported humps in the capacitance-voltage characteristics of QLEDs and attributed these characteristics to the imbalanced carrier injections.^[22] However, the impedance spectroscopy technique has not been fully exploited, and the relevant data has not been thoroughly analyzed. In this work, we clearly demonstrated there were negative charges accumulated in the thin films composed of CdSe/ZnS QDs (from Mesolight Nanotech Co., Ltd.) by conducting impedance spectroscopy on working QLEDs. Strong evidence obtained from electrophoretic deposition (EPD) supported that the sign of the accumulated charges was negative. Positively or negatively charged QDs in solutions were also reported in previous literatures.^[23–25] Through systematically analyzing the capacitance-voltage and capacitance-frequency characteristics of QLEDs with different designs of structures, we elaborated how to determine the sign of the accumulated charges, and how the carrier injections were affected by the QDs with surface charges. Previous works usually estimated the carrier injection barriers by looking at the energy levels of different layers separately without considering the possible interactions between different layers. Therefore, most previous works claimed that there were high potential barriers for hole injection in QLEDs, due to the large gap between the highest unoccupied molecular orbitals (HOMO) of hole transport layer (HTL) and the valence band maximum (VBM) of QDs.^[26–28] On the other hand, there were also a lot of works showing that reducing the gap between the HOMO of HTL and VBM of QDs did not apparently reduce the turn-on voltages of QLEDs, instead, improving hole mobility was more helpful.^[29,30] This inconsistency makes people hesitant to believe there are large potential barriers for hole injection in QLEDs. This work provided reasonable descriptions and proposed explanations on the actual hole and electron dynamics in QLEDs using different types of electron transport layers (ETLs), such as organic ETL and metal oxide ETL.

2. Results and Discussions

Two QLEDs with the device structures shown in **Figure 1a** were fabricated and characterized. Indium tin oxide (ITO) coated glass substrates were used as anodes. By coating poly(3,4-ethylenedioxythiophene) polystyrene sulfonate (PEDOT:PSS) on ITO/glass substrate, holes are easily injected into the organic HTL, Poly(9,9-dioctylfluorene-alt-*N*-(4-sec-butylphenyl)-diphenylamine) (TFB). 2,2'',2'''-(1,3,5-Benzinetriyl)-tris(1-phenyl-1-H-benzimidazole) (TPBi) or zinc oxides (ZnO) were used as ETL in the two QLEDs, respectively. The thicknesses of TFB, red CdSe/ZnS QD layer, TPBi, and ZnO in working devices were about 35, 20, 45, and 30 nm, respectively. The active areas of all the devices in this work were 4 mm². If TPBi was used as ETL, Al combined with 1.2 nm LiF was used as cathode. Figure 1b showed the energy levels of different functional layers if they were separately characterized. QLED with ZnO ETL showed better performance in terms of low turn-on voltage (1.7 V), high luminance, and external quantum efficiency (EQE) as shown in Figure 1c,d, which has been verified by numerous previous works. This was usually explained by that ZnO improved electron injection due to its high electron mobility. More important explanations on ZnO would be discussed at the end of this work. On the other hand, according to numerous reported works about OLEDs and PeLEDs,^[31–34] the barrier for electron injection at TPBi/LiF/Al interface was minimal suggesting the turn-on voltage of the QLEDs with TPBi/LiF/Al should not be significant higher than that of the QLEDs with ZnO/Al. To understand the abnormally high turn-on voltage in QLED with TPBi (3.2 V), we conducted impedance spectroscopy to study the charge injections in QLEDs with different device structures. As shown in Figure 1e, distinct features were observed between the capacitance-voltage (*C*-*V*) characteristics of the QLEDs using ZnO and TPBi as ETL. The *C*-*V* characteristics shown in this work were all measured at 10 kHz if no special instructions

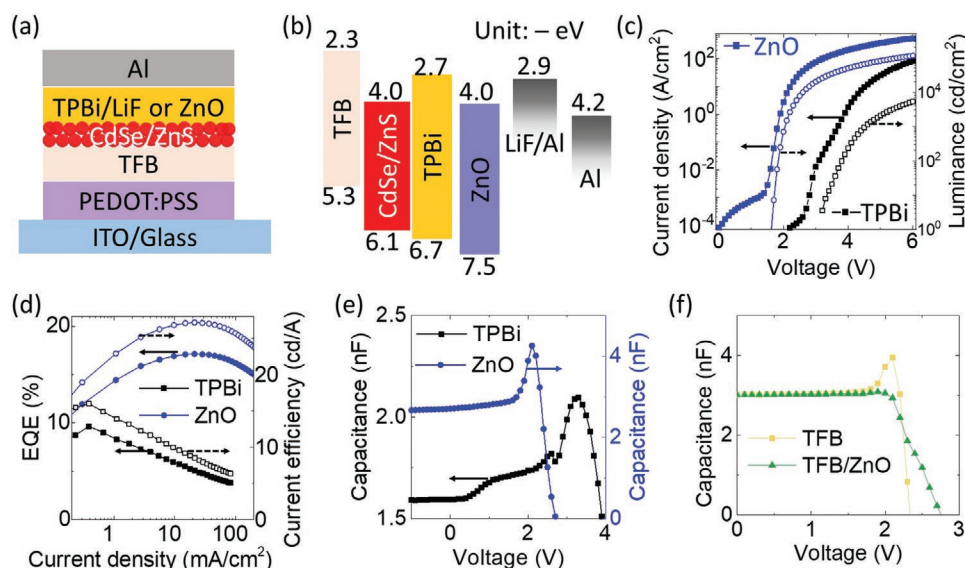


Figure 1. a) Schematics of the device structure; b) Energy levels of some functional layers used in QLEDs; c) Current density-voltage-luminance (*J*-*V*-*L*) characteristics, d) EQEs and current efficiencies, e) Capacitance-voltage (*C*-*V*) characteristics of QLEDs using ZnO and TPBi as ETLs; f) Capacitance-voltage (*C*-*V*) characteristics of devices with structures of ITO/PEDOT:PSS/TFB/Al and ITO/PEDOT:PSS/TFB/ZnO/Al.

mentioned. With 10 kHz AC voltage, there was enough time ($>10\ \mu\text{s}$) for the carrier transport and accumulation (if any) in several tens of nanometer thick organic charge transport layers. Around zero bias, the capacitances were contributed by geometrical capacitance in both devices. The increase of capacitances suggested additional carriers were injected and accumulated in the device, while the decrease of capacitances suggested quenching of carriers through carrier recombination or extraction. As bias increased in the forward direction, the capacitance started to increase at 1.7 V in QLEDs using ZnO ETL, suggesting the carrier injection was initiated at 1.7 V forward bias. This QLED also turned on at around 1.7 V as indicated in Figure 1c. On the other hand, the carrier injection in QLEDs using TPBi ETL started at around 0.5 V, as indicated by their C - V characteristics in Figure 1e. There was another fast increase in capacitance after the forward bias increase to over 2.8 V. The capacitance obtained its peak value at 3.2 V, at which this QLEDs turned on. This meant the carrier injection was initiated well before this QLED turned on. This indicated that the injections of holes and electrons in the QLEDs using TPBi as ETL started at different applied biases. The conclusion would be the electrons were injected at 0.5 V and holes were injected at >2.8 V, according to the prevailing argument that electron injection was much easier than hole injection in QLED. However, our studies with impedance spectroscopy indicated the facts were exactly the opposite. To understand the data from impedance spectroscopy, we first identified which

layers in the devices were able to contribute capacitances in working devices. The layers of PEDOT:PSS, LiF, ITO, and Al cannot contribute capacitances, since they work as conductors/resistors (contributing resistances only) in working devices. Two devices with structures of ITO/PEDOT:PSS/35 nm TFB/Al and ITO/PEDOT:PSS/35 nm TFB/40 nm ZnO/Al were fabricated and characterized by impedance spectroscopy to demonstrate that ZnO layer did not contribute any capacitances, either. As shown in Figure 1f, the geometrical capacitances of the above two devices were exactly the same, i.e., $\approx 3.1\ \text{nF}$, which were exactly equal to the capacitance of a layer of 35 nm TFB (dielectric constant: ≈ 3) with area of $4\ \text{mm}^2$. Therefore, in the following discussions, layers affecting the capacitances only included TFB, QDs, and TPBi layers.

To understand the details of the abnormal carrier injections, a series of devices with different thicknesses of QD layers were fabricated and characterized by impedance spectroscopy. The QD layer cast from $15\ \text{mg mL}^{-1}$ colloidal QD dispersion in octane QLEDs was composed of only 2–3 monolayers of QDs, while QDs cast from $0.5\ \text{mg mL}^{-1}$ dispersion were embedded on the surface of TFB without continuous thin films, as shown in the inset of Figure 2a. The typical J - V - L characteristics of devices with or without QDs were shown in Figure 2a. The double peaks in the spectra of the devices with different amounts of QDs shown in Figure 2b demonstrated that the red emission from QDs were significant even if the QD solution was only $0.5\ \text{mg mL}^{-1}$. As shown in Figure 2, the device

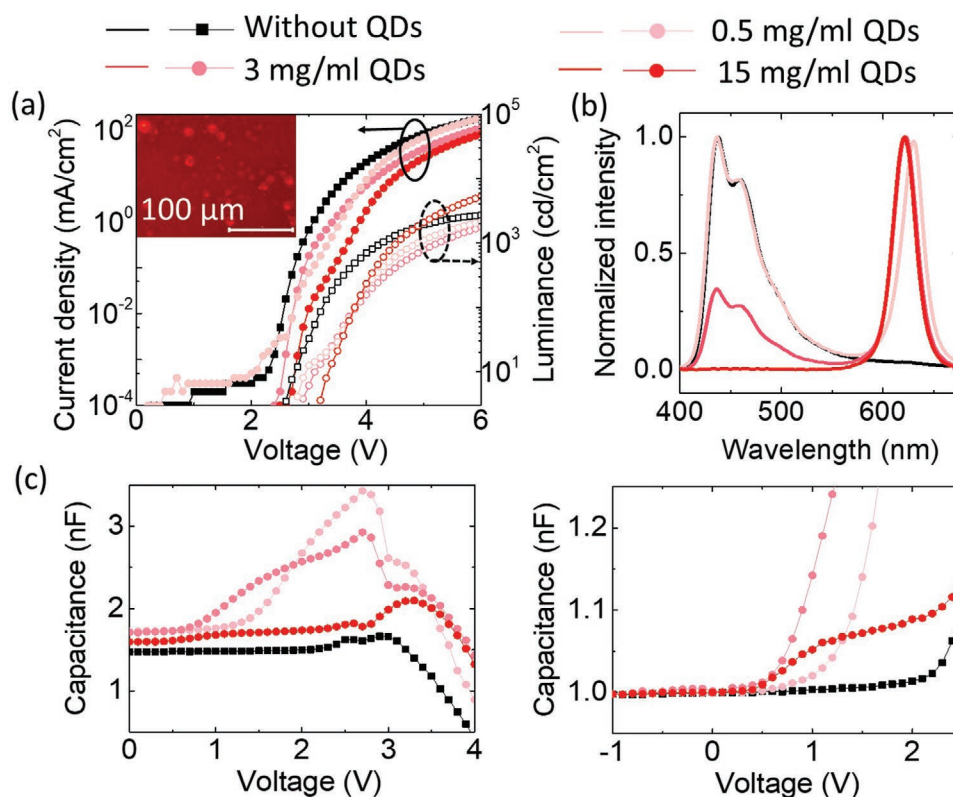


Figure 2. a) J - V - L characteristics of QLEDs with/without QDs, the inset is a microscope photo of QDs on HTL cast from $0.5\ \text{mg mL}^{-1}$ dispersion; b) Normalized electroluminescent (EL) spectra of devices with different thicknesses of QD layers; c) Capacitance-voltage characteristics (with zoom-in part) of the QLEDs with different amount/thicknesses of QDs.

without QDs was turned on at 2.5 V and emitted blue light, and its capacitance started to increase at 2.4 V. This meant that the bipolar injection and radiative recombination almost happened simultaneously. On the other hand, devices with QDs showed larger turn-on voltage (>2.8 V), but their capacitances started to increase at voltages less than 1 V. The region where capacitances started to rise was zoomed in, as shown in Figure 2c. Even a very small amount of QDs in the device made the injection barrier for one type of carriers decreased significantly. Another two significant differences observed on the C–V characteristics between devices with and without ultrathin QDs (0.5 mg mL^{-1} QD and 3 mg mL^{-1} QD) were: (1) the first dramatic decrease of capacitance was overserved (at 2.7 V bias) before the devices with QDs turned on (at 2.9 V bias), while the capacitance started to decrease after the device without QDs turned on; (2) the capacitances at zero bias (i.e., geometrical capacitances) increased a lot in devices with ultrathin QD layer. We proposed the explanations for these abnormal phenomena as: there were charges accumulated on the surfaces of the QDs. The additional surface charges in QDs led to additional induced charges on the electrodes, which explained the increase of the geometrical capacitances observed at zero bias. On the other hand, the accumulated surface charges distorted the energy alignments at the interfaces between charge transport layers and QD layer. As a result, injection of one type of carriers

was promoted, while the other was impeded. Therefore, hole injection and electron injection started at different biases. The decrease of capacitance before the device turned on was due to the recombination (mainly nonradiative) between the firstly injected carriers and the originally accumulated charges in QD layer with minimal light emitted. This kind of recombination quenched more accumulated holes with more charged QDs in the device, leading to a reduction of the peak values of capacitances in Figure 2c as thicker QD layers were included.

The discussions on the experimental results shown in Figure 3 finally draw a conclusion that hole injection started at lower bias, while electron injection started at higher bias in these QLEDs. The equivalent resistance–capacitance (RC) circuit shown in Figure 3a was usually used to analyze the charge dynamics in electronic devices.^[17,35,36] Units of R_1C_1 and R_2C_2 represented TFB layer and TPBi layer, respectively. Another series of QLEDs with 0.5 mg mL^{-1} QDs were fabricated, in which the carrier quenching caused by the traps on QDs were minimized. The thicknesses of TFB and TPBi layers were systematically varied as indicated by the plot legends in Figure 3b. When the capacitance–frequency (C–f) characteristics were measured at zero bias without any carrier injection, the capacitance kept constant (geometrical capacitance) until the frequency approached to 1 MHz. When the devices were characterized at 2.5 V forward bias, abrupt changes in capacitances

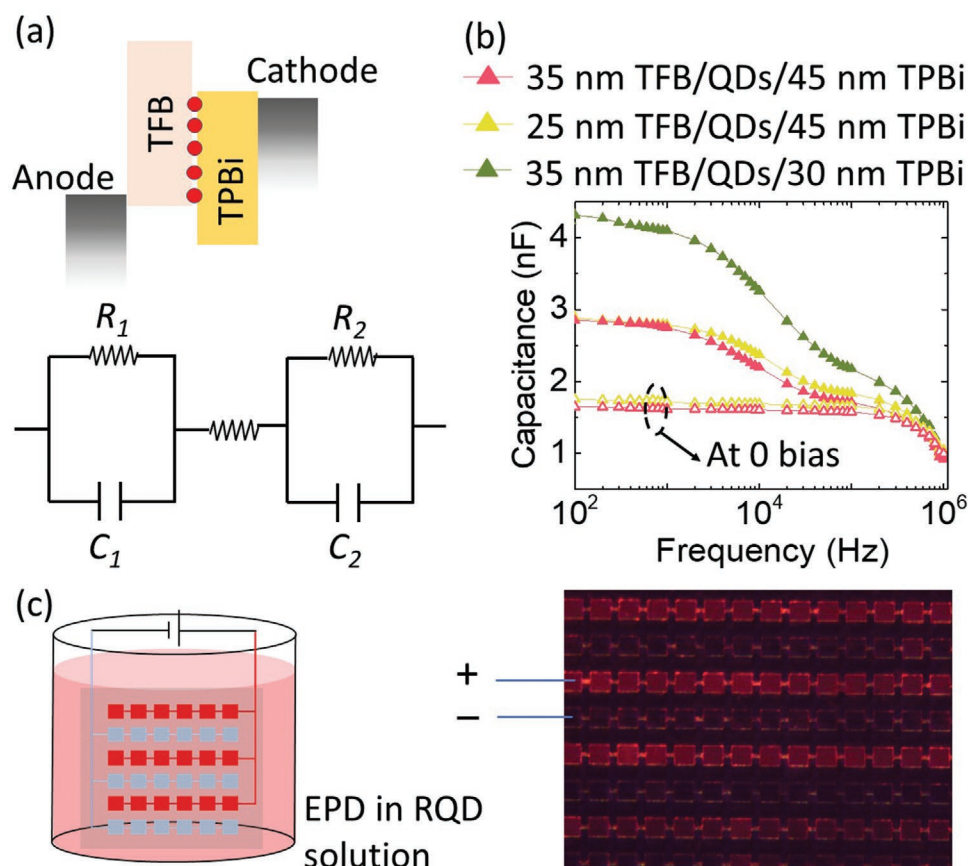


Figure 3. a) The device structure of QLEDs and its equivalent RC circuit; b) C–f characteristics of the QLEDs with different thicknesses of TFB and TPBi layers, measured at 2.5 V bias (solid symbols) or zero bias (hollow symbols); c) The schematics for the set-up of EPD and microscope image showing the patterned red QDs films deposited by EPD.

were observed at intermediate frequencies. With 2.5 V bias, only one type of carriers was injected, so that there was no significant radiative recombination. Therefore, in all the impedance measurements, the discrete QDs did not significantly affect the quenching of carriers, suggesting that they can be regarded as resistor or conductor in the equivalent circuit. If frequency was high enough so that the injected carriers did not get the time ($>10\ \mu\text{s}$) to be transported and accumulated at HTL/QD or ETL/QD interfaces, the capacitance of this RC circuit was approximately $C_1C_2/(C_1+C_2)$, which was inversely proportional to the total thickness of TFB and TPBi. The total thicknesses of TFB and TPBi in the three QLEDs were 80, 70, and 65 nm, respectively. Correspondingly, the capacitances at high frequency (approaching 1 MHz) of the three QLEDs shown in Figure 3b were consistent with the above theoretical analysis. On the other hand, large amounts of carriers were efficiently transported through HTL or ETL at low frequency ($<1\ \text{kHz}$) and accumulated at the space close to the interface between transport layer and QDs. In this case, one of the transport layers (R_1C_1 or R_2C_2 unit) mainly behaved like a conductor, making the capacitor parallel to it nearly short-circuited. The capacitance approximately equaled to C_1 only or C_2 only. Through comparisons between the C - f characteristics of the three devices shown in Figure 3b, the capacitance measured with 2.5 V bias and at low frequency was determined by the thickness of TPBi, rather than TFB. More precisely, the capacitance increased from 2.9 to 4.3 nF (≈ 1.5 times) when the thickness of TPBi decreased from 45 to 30 nm ($1/1.5$ times). On the other side, the thickness of TFB layer didn't make any differences to the capacitances at low frequency. This indicated that TFB layer become a conductor due to high concentration of transported carriers, while TPBi layer was still a dielectric layer due to no injection of

electrons at 2.5 V bias. Therefore, we concluded that hole injection started at lower bias ($<1\ \text{V}$), while electron injection started at higher bias ($\approx 3\ \text{V}$). The origin of this abnormal injection of carriers was attributed to the intrinsic negative charges accumulated in the QD layer, which reduced the hole injection barrier via Coulombic attraction.

The QD layer may accumulate negative or positive charges depending on the synthetic routes for QD colloidal suspension.^[23–25] Our analysis based on impedance spectroscopy suggested the accumulated charges were negative. EPD was conducted to verify and support this conclusion. The description of EPD experiment and results were shown in Figure 3c. Patterned electrodes were made on the substrate first. Pixels in the same line were connected together to work as anode or cathode. Positive bias ($\approx 60\ \text{V}$) was applied to the anode after the substrate immersed into red CdSe/ZnS QD solution. Kept the bias for about 3 min before the substrate was lifted up and observed under optical microscope. As shown in Figure 3c, the red QDs were mainly deposited on the electrodes with positive bias, which suggested the QDs in the solution were mainly driven towards the high potential side. This was a strong and direct evidence for the existence of negative charges on the QD surface.

The schematic picture shown in Figure 4a–c helped to get the physical intuition of the relationship between the abnormal charge injection in QLED and the negative accumulated charges in QD layer. As shown in Figure 4a, when the external bias increased to be equal to the built-in potential, or the work function differences between ITO/PEDOT:PSS anode and LiF/Al cathode, flat band condition was achieved in the device if there was no other factors contributing additional electric field. At flat band condition, the total electric-field (E -field) in

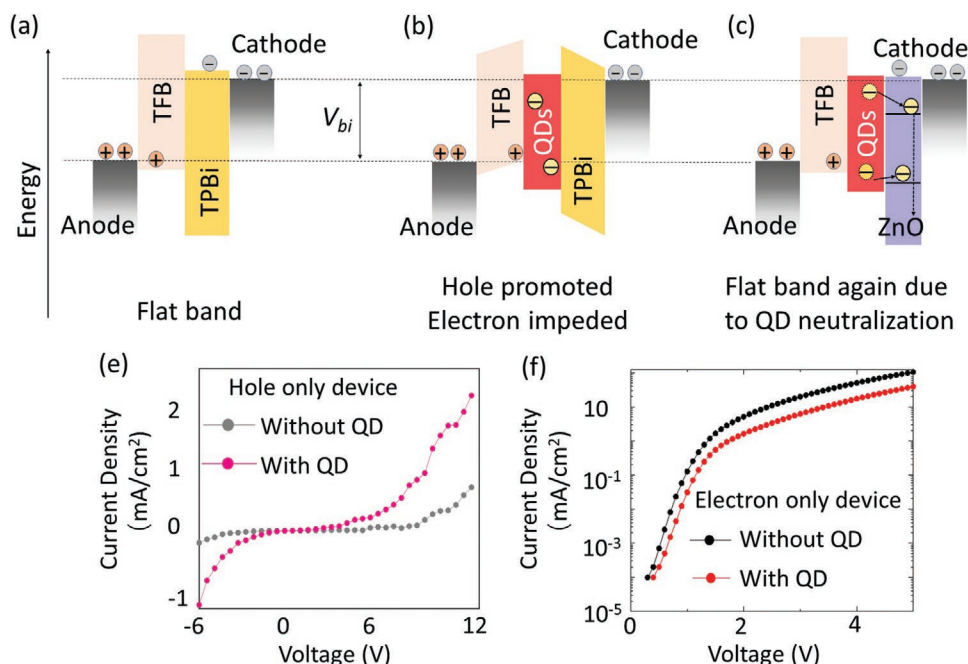


Figure 4. a–c) Schematic diagrams of the energy alignment and charge dynamics in a) devices without QDs, b) QLEDs with negatively charged QDs and TPBi ETL, and c) QLEDs with negatively charged QDs and ZnO ETL; e,f) J - V characteristics of hole and electron only device with or without charged QDs.

TFB and TPBi layers were zero. Previous works demonstrated that the contact PEDOT:PSS/TFB, and TPBi/LiF/Al are nearly Ohmic.^[37–39] Therefore, under flat band condition, holes and electrons were simultaneously injected into the TFB layer and TPBi layer. The scenario of energy level alignments and charge dynamics in the devices was dramatically different if QDs carried negative charges. As shown in Figure 4b, the device was not in flat band condition even if the external bias exactly canceled out the built-in potential. Due to the negative charges in QD layer, hole injection was accelerated, while electron injection was rejected. As a result, the holes were injected into TFB and transported efficiently at very low forward bias, while the electron still accumulated at the TPBi/cathode interface at high bias (>2.5 V), leaving the TPBi layer alone contributing to the capacitance of the device. The above analysis clearly explained our observation that hole and electron injections started at different applied bias. Hole only and electron only devices were fabricated to confirm the effects on hole and electron injection caused by the charged QDs. The structure of the hole only devices were ITO/PEDOT:PSS/TFB/with or without QDs/CBP/MoO₃/Al, where CBP was hole transport material with full name as 4,4'-Bis (N-carbazolyl)-1,1'-biphenyl. The structure of the electron only devices were Al/with or without QDs/TPBi/LiF/Al. The *J*-*V* characteristics of the hole and electron only devices were shown in Figure 4e,f. It indicated that the hole current was improved, while the electron current was suppressed by including an ultrathin layer of charged QD film.

There was previous work showing that the electrons and holes were injected into the QD layer sequentially even if the QDs were neutral at the initial states.^[6,7] That work also suggested that once an electron was injected into a QD and the QD was negatively charged, then the barrier for the subsequent hole injection was greatly reduced.^[6,7] However, in our work, the recombination between the original existed negative charges and the injected holes in QLED using TPBi as ETL did not generate significant light emission at bias of 2.5–3.2 V. Therefore, the initial negative charges mainly led to nonradiative loss. This suggested that the initial charges in the QD layer were more likely trapped charges rather than free electrons in conduction band, though the physical nature of the them were not clear yet. If TPBi was replaced by ZnO, the charge dynamics changed significantly again, due to the distinct electronic properties between organic ETL and oxide semiconductors. It was commonly accepted that the rich trap states in the mid band gap of ZnO were responsible for the large amounts of free electrons in the conduction band of ZnO.^[40] It was highly possible that the energy levels of the trapped electrons in QDs were very similar to those of some mid gap states in ZnO. This facilitated the transfer of the trapped charges from QDs to ZnO, leading to charge neutralization in QD layer. The charge neutralization in QD layer due to the spontaneous charge transfer between ZnO and QDs was also observed in previous work.^[41,42] Whereafter, the electrons trapped in ZnO were either thermally activated into the conduction band and become free carriers, or relaxed to ground states in ZnO. After the QDs were neutralized by ZnO, the electron injection become highly efficient. Nanometer-scale ZnO behaved more like a conductor and did not contribute capacitance to the whole devices, due to the large amounts of free carriers in ZnO and smooth electron transfer

between QDs, ZnO, and Al electrodes. Due to the much higher degeneracy of conduction band compared to that of the deep trap states in QD layer, the injected electrons are more likely to be coupled into the conduction band, and it takes long time to fill the deep traps. Therefore, the injected electrons in QDs mainly stayed in conduction band, resulting in efficient radiative recombination with subsequently injected holes and a low turn-on voltage of 1.7 V. This mechanism about charge dynamics in QLEDs with ZnO ETL also lead to significant enhancement of quantum efficiency and current efficiency.

3. Summary and Conclusion

The carrier injection and charge transfer at interfaces in QLEDs were commonly evaluated by examining the energy levels of different functional layers. However, the carrier injection and charge transfer may be distinct from the expectation given by this kind of evaluation. The *C*-*V* characteristics of a series QLED devices revealed that holes and electrons were injected at different applied bias if TPBi was used as ETL, while they are happened at the same bias if ZnO was used as ETL. More in-depth analysis on the results got from impedance spectroscopy suggested that the negative accumulated charges in QD layer were responsible for the hole and electron injection at different applied bias in the QLEDs with TPBi as ETL. Results from EPD also strongly supported the existence of intrinsic negative charges in QD layer. The hole injection may start at a bias as low as 0.5 V. However, the injected holes did not generate significant light emission through recombination with the original accumulated negative charges. The physical nature of the accumulated negative charges in QD layer deserved further investigation. On the other hand, the adverse impacts of the accumulated charges can be mitigated by replacing TPBi with ZnO. The QD layer was neutralized due to the matched mid gap states with the energy states of the trapped charges in QDs, and smooth transfer of electrons between QDs, ZnO, and Al electrodes. After all, including more charge dynamic processes in QLEDs leads to less reliability and higher chances of energy loss. Though high performance QLEDs using ZnO as ETL were frequently reported, applying QLED in industrial products still faces some challenges about reliability, repeatability, and too stringent requirements on fabrication processes. Neutral QDs without accumulated charges and better control of charge dynamics at the HTL/QD and QD/ETL interfaces are highly desired for fabrication of reliable electroluminescent devices.

4. Experimental Section

Red CdSe/ZnS QDs and ZnO nanoparticles were purchased from Suzhou Xingshuo Nanotech Co., Ltd. Devices with structure of glass/ITO/PEDOT:PSS (45 nm)/TFB/ QDs/ TPBi/ LiF (1.2 nm)/Al (100 nm) or glass/ITO/PEDOT:PSS (45 nm)/TFB/ QDs/ ZnO (40 nm)/Al (100 nm) were fabricated. The sheet resistance of the ITO glasses was 20 Ω sq⁻¹. The glass/ITO substrates were cleaned with detergent, deionized water, and isopropanol in ultrasonic for 20 min each, followed by oxygen plasma treatment for 10min. Then the PEDOT:PSS (Clevios Al 4083) layer was spin-cast at 3000 rpm for 45 s onto the precleaned ITO-substrate, and then annealed at 130 °C for 15 min in the air. The substrates were then transferred to a nitrogen-filled glove box. 35 nm

TFB and 25 nm TFB layer on top of the PEDOT:PSS layer were spin-cast from 8 and 6 mg mL⁻¹ solution in chlorobenzene with spin speed of 4000 rpm, respectively. The TFB layers were annealed at 120 °C for 10 min. The QD layer with different thicknesses was spin-cast from 15, 3, and 0.5 mg mL⁻¹ QD dispersions in octane, respectively. ZnO layer was spin-cast from 20 mg mL⁻¹ ZnO nanoparticle dispersion in ethanol. TPBi, LiF, and Al were thermally deposited in a vacuum chamber with pressure smaller than 6×10^{-4} Pa and the devices were encapsulated using a cover glass and a UV-curable epoxy. The thicknesses of the functional layer were measured by using a Bruker DektakXT Stylus Profiler. The current density–voltage (*J*–*V*) characteristics were recorded by a programmable source meter (Keithley 2614B). The forward direction photons emitted from the devices were detected by a calibrated UDT PIN-25D silicon photodiode. The characteristics about impedance spectroscopy were obtained from an HP 4284A impedance analyzer.

Acknowledgements

The authors would like to acknowledge support from the Ministry of Science and Technology of China (No. 2016YFB0401702), National Natural Science Foundation of China (Nos. 62005114, 62005115, 61674074, 61875082), Guangdong Province's Key R&D Program: Micro-LED Display and Ultra-high Brightness Micro-display Technology (Project No. 2019B010925001); Environmentally Friendly Quantum Dots Luminescent Materials (Project No. 2019B010924001), Guangdong Basic and Applied Basic Research Foundation (Project No. 2019A1515110437), Guangdong Youth Innovative Talents Project (No. 2018KQNCX228), Shenzhen Peacock Team Project (No. KQTD2016030111203005), and Shenzhen Innovation Project (No. JCYJ20180305180629908).

Conflict of Interest

The authors declare no conflict of interest.

Data Availability Statement

Research data are not shared.

Keywords

charge dynamics, charge neutralization, impedance spectroscopy, quantum-dot light-emitting diodes, surface charges

Received: February 23, 2021

Revised: May 7, 2021

Published online:

- [1] X. Dai, Z. Zhang, Y. Jin, Y. Niu, H. Cao, X. Liang, L. Chen, J. Wang, X. Peng, *Nature* **2014**, 515, 96.
- [2] H. Zhang, X. Sun, S. Chen, *Adv. Funct. Mater.* **2017**, 27, 1.
- [3] H. Zhang, S. Chen, X. W. Sun, *ACS Nano* **2018**, 12, 697.
- [4] L. Wang, J. Lin, Y. Hu, X. Guo, Y. Lv, Z. Tang, J. Zhao, Y. Fan, N. Zhang, Y. Wang, X. Liu, *ACS Appl. Mater. Interfaces* **2017**, 9, 38755.
- [5] H. Qin, R. Meng, N. Wang, X. Peng, *Adv. Mater.* **2017**, 29, 1606923.
- [6] W. Xu, X. Hou, Y. Meng, R. Meng, Z. Wang, H. Qin, X. Peng, X. W. Chen, *Nano Lett.* **2017**, 17, 7487.
- [7] X. Lin, X. Dai, C. Pu, Y. Deng, Y. Niu, L. Tong, W. Fang, Y. Jin, X. Peng, *Nat. Commun.* **2017**, 8, 1.

- [8] W. Zhang, W. Zhuang, R. Liu, X. Xing, X. Qu, H. Liu, B. Xu, K. Wang, X. W. Sun, *ACS Omega* **2019**, 4, 18961.
- [9] Z. Wu, P. Liu, W. Zhang, K. Wang, X. W. Sun, *ACS Energy Lett.* **2020**, 5, 1095.
- [10] Y. Won, O. Cho, T. Kim, D. Chung, T. Kim, H. Chung, H. Jang, J. Lee, D. Kim, E. Jang, *Nature* **2019**, 575, 634.
- [11] W. Ji, Y. Lv, P. Jing, H. Zhang, J. Wang, H. Zhang, J. Zhao, *ACS Appl. Mater. Interfaces* **2015**, 7, 15955.
- [12] H. Moon, W. Lee, H. Chae, *IEEE Electron Device Lett.* **2019**, 40, 1872.
- [13] J. Lim, M. Park, W. K. Bae, D. Lee, S. Lee, C. Lee, K. Char, *ACS Nano* **2013**, 7, 9019.
- [14] Y. Deng, X. Lin, W. Fang, D. Di, L. Wang, R. H. Friend, X. Peng, Y. Jin, *Nat. Commun.* **2020**, 11, 1.
- [15] W. Zhang, S. Ding, W. Zhuang, D. Wu, P. Liu, X. Qu, H. Liu, H. Yang, Z. Wu, K. Wang, X. W. Sun, *Adv. Funct. Mater.* **2020**, 2005303, 1.
- [16] S. Nowy, W. Ren, A. Elschner, W. Lövenich, W. Brütting, *J. Appl. Phys.* **2010**, 107, 054501.
- [17] P. Chulkin, O. Vybornyi, M. Lapkowski, P. J. Skabara, P. Data, *J. Mater. Chem. C* **2018**, 6, 1008.
- [18] Q. Zhang, X. Zhang, B. Wei, *Optik (Stuttg)* **2015**, 126, 1595.
- [19] T. Okachi, T. Nagase, T. Kobayashi, H. Naito, *Jpn. J. Appl. Phys.* **2008**, 47, 8965.
- [20] A. Uddin, C. C. Teo, *Appl. Phys. A: Mater. Sci. Process.* **2011**, 105, 39.
- [21] C. Blauth, P. Mulvaney, T. Hirai, *J. Appl. Phys.* **2019**, 125, 195501.
- [22] K. Lee, J. Yun, S. Lee, J. Song, Y. Kim, J. Kwak, G. T. Kim, *Nanoscale* **2020**, 12, 15888.
- [23] K. Wu, Y. S. Park, J. Lim, V. I. Klimov, *Nat. Nanotechnol.* **2017**, 12, 1140.
- [24] I. M. R. Moura, P. E. Cabral Filho, M. A. B. L. Seabra, G. Pereira, G. A. L. Pereira, A. Fontes, B. S. Santos, *J. Lumin.* **2018**, 201, 284.
- [25] W. Qin, H. Liu, P. Guyot-Sionnest, *ACS Nano* **2014**, 8, 283.
- [26] Y. Lei, Y. Zhao, Q. Zhang, Z. Xiong, L. Chen, *Org. Electron.* **2020**, 81, 105683.
- [27] D. Dong, F. Zhu, S. Wu, L. Lian, H. Wang, D. Xu, G. He, *Org. Electron.* **2019**, 68, 22.
- [28] J. Kwak, W. K. Bae, D. Lee, I. Park, J. Lim, M. Park, H. Cho, H. Woo, D. Y. Yoon, K. Char, S. Lee, C. Lee, *Nano Lett.* **2012**, 12, 2362.
- [29] M. D. Ho, D. Kim, N. Kim, S. M. Cho, H. Chae, *ACS Appl. Mater. Interfaces* **2013**, 5, 12369.
- [30] X. Zhang, H. Dai, J. Zhao, S. Wang, X. Sun, *Thin Solid Films* **2016**, 603, 187.
- [31] S. H. Jeong, S. H. Woo, T. H. Han, M. H. Park, H. Cho, Y. H. Kim, H. Cho, H. Kim, S. Yoo, T. W. Lee, *NPG Asia Mater.* **2017**, 9, e411.
- [32] S. Kumar, J. Jagielski, N. Kallikounis, Y. H. Kim, C. Wolf, F. Jenny, T. Tian, C. J. Hofer, Y. C. Chiu, W. J. Stark, T. W. Lee, C. J. Shih, *Nano Lett.* **2017**, 17, 5277.
- [33] M. K. Gangishetty, S. Hou, Q. Quan, D. N. Congreve, *Adv. Mater.* **2018**, 30, 1.
- [34] X. Zhang, H. Lin, H. Huang, C. Reckmeier, Y. Zhang, W. C. H. Choy, A. L. Rogach, *Nano Lett.* **2016**, 16, 1415.
- [35] Z. Wu, Y. Zhai, W. Yao, N. Eedugurala, S. Zhang, L. Huang, X. Gu, J. D. Azoulay, T. N. Ng, *Adv. Funct. Mater.* **2018**, 28, 1.
- [36] G. Paasch, S. Scheinert, *Synth. Met.* **2001**, 122, 145.
- [37] Z. Wu, W. Yao, A. E. London, J. D. Azoulay, T. N. Ng, *Adv. Funct. Mater.* **2018**, 28, 1.
- [38] Z. Wu, B. Wu, H. L. Tam, F. Zhu, *Organic Electronics* **2016**, 31, 266.
- [39] L. S. Hung, C. W. Tang, M. G. Mason, P. Raychaudhuri, J. Madathil, *Appl. Phys. Lett.* **2001**, 78, 544.
- [40] A. Janotti, C. G. Van De Walle, *Rep. Prog. Phys.* **2009**, 72, 126501.
- [41] B. S. Mashford, M. Stevenson, Z. Popovic, C. Hamilton, Z. Zhou, C. Breen, J. Steckel, V. Bulovic, M. Bawendi, S. Coe-Sullivan, P. T. Kazlas, *Nat. Photonics* **2013**, 7, 407.
- [42] K. Tvrđy, P. A. Frantsuzov, P. V. Kamat, *Proc. Natl. Acad. Sci. USA* **2011**, 108, 29.